Narrowband and ultra-wideband modulation instability in nonlinear metamaterial waveguides

N. Linale,[1, 4, *] P. I. Fierens,[2, 4] S. M. Hernandez,[3] J. Bonetti,[1, 4] and D. F. Grosz[1, 4]

[1] *Depto. de Ingeniería en Telecomunicaciones, Centro Atómico Bariloche, Comisión Nacional de Energía Atómica, Río Negro 8400, Argentina*

[2] *Grupo de Optoelectrónica, Instituto Tecnológico de Buenos Aires (ITBA), CABA 1106, Argentina*

[3] *Instituto Balseiro, Universidad Nacional de Cuyo, Bariloche, Río Negro 8400, Argentina*

[4] *Consejo Nacional de Investigaciones Científicas y Técnicas (CONICET), Argentina*

[*] *nicolas.linale@cab.cnea.gov.ar*

Abstract: Waveguides based on metamaterials may exhibit strongly frequency-dependent nonlinearities. In this work, we focus on the phenomenon of modulation instability in this type of waveguides, departing from a new modeling equation that ensures strict conservation of both the energy and the photon number of the parametric process. In particular, we analyse the case of a waveguide with a linearly frequency-dependent nonlinear coefficient, revealing unique features such as narrowband and ultra-wideband gain spectra, and the suppression of the power cutoff giving rise to an ever-growing MI gain. These markedly distinct regimes are enabled by self-steepening (SS) and manifest themselves depending upon the magnitude and sign of the SS parameter. We believe these findings to be most relevant in the context of mid-IR supercontinuum sources.

1. Introduction

Modulation instability (MI) is a four-wave mixing process by which two photons from a pump at frequency ω_0 are annihilated, and two photons at $\omega_0 \pm \Delta\omega$ are created. MI, which has been widely discussed in the literature [1–7], manifests itself as a gain in frequency bands at both sides of the pump which are most relevant, *e.g.*, in the initial stages of soliton formation and supercontinuum generation, and finds applications in a vast number of areas in science [8, 9].

In particular, modulation instability depends on the frequency response of the nonlinear waveguide. The simplest model assumes a linear frequency dependence of the nonlinear coefficient, γ, such that $\gamma(\Omega) = \gamma_0 + \gamma_1\Omega$, where Ω is the deviation from a central frequency ω_0. The linear term of $\gamma(\Omega)$ is responsible for self-steepening (SS), a nonlinear process that produces the steepening and subsequent shock of optical pulses [10]. It has been proved that, in the presence of SS, there exists a cutoff power (COP) above which the MI gain vanishes; as such, the COP poses a limit to the maximum attainable gain and bandwidth of MI sidebands. The presence of a cutoff power and the dependence of the MI gain with pump power and frequency were first reported by Shukla and Rasmussen [11] and De Angelis *et al.* [12] in the context of the nonlinear Schrödinger equation (NLSE). Additionally, Hernandez *et al.* [6] presented a geometrical model explaining the dependence of both the MI gain and the COP with higher-order dispersion.

Analyses in Refs. [6, 11–14] are based on the particular case where $\gamma_0 > 0$ and $\gamma_1 = \gamma_0/\omega_0$. Both conditions are lifted in the work of Wen and colleagues [15, 16] where negative-index metamaterials (NIM) are analyzed. The authors show that self-steepening can be engineered in NIMs and thus MI can be manipulated [15]. Moreover, they report an MI-gain decrease and the shrinking of the gain band due to SS, and observe that MI in NIMs is independent of the sign of the self-steepening parameter γ_1 [15]. Contrary to this last observation, in this paper we show that the sign of the SS parameter has important consequences in both the MI gain and COP.

The difference between our results and those in Refs. [15, 16] stems from two facts. On the one hand, Wen and colleagues do not consider the influence of the frequency dependence of the third order susceptibility $\chi^{(3)}$, and the self-steepening parameter originates in other properties of the material. On the other hand, modeling equations in Refs. [15, 16], although probably adequate for some applications, do not preserve certain physical magnitudes. Indeed, even in lossless media the NLSE only conserves the energy and the number of photons in some particular cases [17]. Blow and Wood [18] showed that if both magnitudes are to be conserved, the nonlinear dispersion in the NLSE must satisfy $\gamma_1 = \gamma_0/\omega_0$, imposing a strong limitation to the nonlinear profiles that can be correctly modeled with the NLSE [19].

Recently, we introduced a modified equation that conserves both the energy and the number of photons, the photon-conserving NLSE (pcNLSE) [19], capable of modeling propagation in waveguides with arbitrary frequency-dependent nonlinear coefficients. Such nonlinear profiles can be found, for instance, in waveguides doped with metal nanoparticles (MNPs). These waveguides may exhibit a zero-nonlinearity wavelength (ZNW) in the near infrared region, leading to new exciting phenomena [20, 21]. Moreover, in our recent work [22] we derived the MI gain as obtained from a linear stability analysis of the pcNLSE, arriving at results departing significantly from those obtained with the NLSE, such as a gain bandwidth extending beyond the zero-nonlinear wavelength and a complex structure of the MI gain. In this paper, we extend the work in Ref. [22] by way of a thorough analysis of the incidence of the self-steepening parameter (in both magnitude and sign) on the MI gain and its bandwidth and derive, for the first time to the very best of our knowledge, an expression for the COP for arbitrary frequency-dependent nonlinear profiles. Moreover, we identify narrowband and ultra-wideband spectral regions, and find striking differences in the waveguide output in the time domain for these two novel regimes. In order to simplify the analysis, we shall limit our study to the case of a linear frequency-dependent nonlinear coefficient. However, this simplification is not overly restrictive since the zero and first-order approximations are the most widely adopted in the literature. Indeed, the linear frequency dependence of $\gamma(\Omega)$ has proved to be adequate to model the propagation of few-cycle pulses [23] and supercontinuum generation spanning over 100 THz [24].

The remaining of this paper is organized as follows. In Section 2 we review the power cutoff for the MI gain in the context of the nonlinear Schrödinger equation, and extend results in previous works in order to account for arbitrary values of the self-steepening parameter. In Section 3 we introduce the photon-conserving NLSE and study the geometry of the MI gain in the frequency-power plane. In particular, we focus on the influence of the SS parameter, showing that it can lead to both narrowband or ultra-wideband gain spectra and the suppression of the power cutoff. Finally, we summarize results in Section 4.

2. Geometrical considerations on the MI gain profile under the NLSE

The nonlinear Schrödinger equation is widely used to model the propagation of light in nonlinear optical fibers. In the frequency domain it reads [25]

$$\frac{\partial \tilde{A}}{\partial z} = i\beta(\Omega)\tilde{A} + i\gamma(\Omega)\mathcal{F}\left[|A|^2 A\right], \tag{1}$$

where $A = A(z,t)$ is the complex envelope of the electric field in the time domain, normalized such that $|A|^2$ is the optical power, Ω is the deviation from an adequate reference frequency ω_0, and $\tilde{A} = \tilde{A}(z,\Omega) = \mathcal{F}[A(z,t)]$ where $\mathcal{F}$ stands for the Fourier transform. Coefficients $\beta(\Omega)$ and $\gamma(\Omega)$ are the linear and nonlinear dispersion profiles, respectively, and it is customary to express these profiles as Taylor expansions. For the sake of simplicity, we shall focus on low order expansions, *i.e.*, $\beta(\Omega) = \beta_2\Omega^2/2$ and $\gamma(\Omega) = \gamma_0 + \gamma_1\Omega$. In the lossless case, $\beta_2, \gamma_0, \gamma_1 \in \mathbb{R}$. It must be observed that, as it was already proved in Ref. [18], the number of photons is conserved

by the NLSE *if and only if* $\gamma_1 = \gamma_{1,\mathrm{pc}} \doteq \gamma_0/\omega_0$. This strict requirement severely impairs the application of the nonlinear Schrödinger equation to more involved nonlinear profiles.

A complete study of the modulation instability gain profile under the NLSE can be found in Refs. [6, 11, 12]. Let us briefly summarize the main results related to the cutoff power of the MI gain. The usual analysis of MI proceeds with a linear stability study of a strong pump, with power P_0 and central frequency ω_0 ($\Omega = 0$), under the effect of small perturbations. It can be shown that these perturbations experience a gain given by

$$g_{\mathrm{MI}}(\Omega) = 2\left|\mathrm{Im}\left\{\sqrt{\left(\frac{\Delta k}{2}\right)^2 - \gamma(\Omega)\gamma(-\Omega)P_0^2}\right\}\right|, \tag{2}$$

where

$$\Delta k = 2k_{\mathrm{P}} - k_{\mathrm{S}} - k_{\mathrm{AS}}, \tag{3}$$

$$\begin{cases} 2k_{\mathrm{P}} &= 2\gamma_0 P_0, \\ k_{\mathrm{S}} &= \beta(-\Omega) + 2\gamma(-\Omega)P_0, \\ k_{\mathrm{AS}} &= \beta(+\Omega) + 2\gamma(\Omega)P_0. \end{cases} \tag{4}$$

From Eq. 2 it is clear that there can only be gain in the region of the (Ω, P_0) plane given by

$$R_{\mathrm{MI}} = \left\{(\Omega, P_0) :\ \Delta k^2 - 4\gamma(\Omega)\gamma(-\Omega)P_0^2 < 0\right\}. \tag{5}$$

A thorough analysis of this region was presented by Hernandez *et al.* [6], including a detailed study of the effect of higher-order dispersion, where only the even terms in the expansion of $\beta(\Omega)$ are shown to have bearing on the MI gain spectrum. For the sake of clarity, we shall not consider the effect of higher-order linear dispersion here and focus on the aforementioned simplified linear and nonlinear coefficients. Under these assumptions, the region of modulation instability gain is given by

$$R_{\mathrm{MI}} = \left\{(\Omega, P_0) :\ \gamma_1^2\Omega^2 P_0^2 + \gamma_0\beta_2\Omega^2 P_0 + \frac{\beta_2^2\Omega^4}{4} < 0\right\}. \tag{6}$$

Moreover, let us write $\gamma_1 = s\gamma_{1,\mathrm{pc}}$, where $s \in \mathbb{R}$ may introduce a deviation from the photon-conserving case in the NLSE (*i.e.*, $s = 1$). Then, whenever $s \neq 0$, the gain boundary can be written as

$$P^{\mathrm{co}} = \hat{P} \times \frac{1 \pm \sqrt{1 - s^2\bar{\Omega}^2}}{s^2}, \tag{7}$$

where $\bar{\Omega} = \Omega/\omega_0$ and

$$\hat{P} = -\frac{\gamma_0\beta_2}{2\gamma_{1,\mathrm{pc}}^2}. \tag{8}$$

Equations 7-8 predict that there will be gain whenever $\gamma_0\beta_2 < 0$ and $|\bar{\Omega}| < 1/|s|$. Moreover, there is a power cutoff beyond which the gain vanishes. Even more interesting is the fact that Eq. 7 predicts that the boundary of the MI region does not depend on the sign of s. That is, whether the nonlinear coefficient $\gamma(\Omega)$ increases or decreases with frequency has not bearing on the boundary of the MI gain region in the (Ω, P_0) plane. This seemingly unintuitive result may stem from the fact that the NLSE does not conserve the number of photons when $s \neq 1$.

Figure 1 shows the MI gain in the (Ω, P_0) plane for two different values of s. Waveguide parameters are set to $\beta_2 = -0.1$ ps^2/km and $\gamma_0 = 1000$ W^{-1}km^{-1}, and the pump wavelength is fixed at 850 nm. Observe that, as s increases, the maximum cutoff power and the MI bandwidth decrease, as predicted by Eqs. 7-8. In particular, the NLSE predicts a decrease in the COP with the square of s and a linear decrease in the gain bandwidth. However, and as it will be shown next, results obtained with the pcNLSE depart substantially from these.

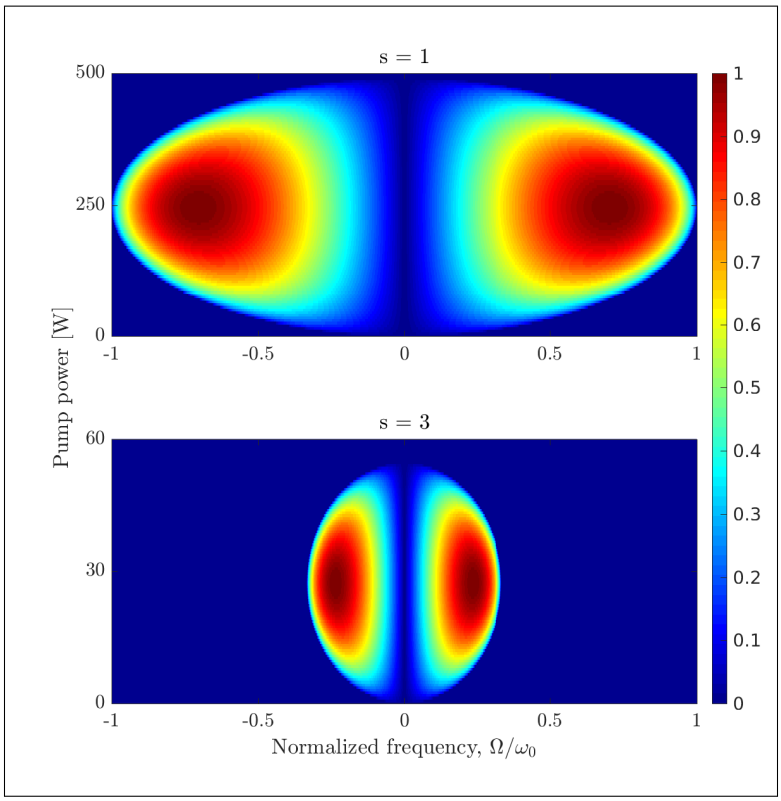

Fig. 1. MI gain for the NLSE with (top) $s = 1$ and (bottom) $s = 3$. Waveguide parameters are $\beta_2 = -0.1$ ps^2/km and $\gamma_0 = 1000$ W^{-1}km^{-1}, and the pump wavelength is 850 nm. Note the reduced COP and bandwidth in the bottom panel.

3. Modulation instability in the photon-conserving NLSE

As it was already stated, the NLSE fails to capture some basic physical properties, such as the conservation of the number of photons of the parametric process, therefore producing unphysical results when dealing with an arbitrary nonlinear profile $\gamma(\Omega)$. Based on basic quantum mechanical considerations, we have recently introduced the photon-conserving nonlinear Schrödinger equation (pcNLSE). In the frequency domain, this equation reads [19]

$$\frac{\partial \tilde{A}}{\partial z} = i\beta(\Omega)\tilde{A} + i\overline{\Gamma}(\Omega)\mathcal{F}\left(C^* B^2\right) + i\overline{\Gamma}^*(\Omega)\mathcal{F}\left(B^* C^2\right), \tag{9}$$

where $\tilde{A}$ is the Fourier transform of the complex envelope A, $\tilde{B} = \sqrt[4]{\gamma(\Omega)/(\Omega+\omega_0)}\tilde{A}$, $\tilde{C} = \left(\sqrt[4]{\gamma(\Omega)/(\Omega+\omega_0)}\right)^* \tilde{A}$, and the effective nonlinear coefficient is $\overline{\Gamma}(\Omega) = \sqrt[4]{\gamma(\Omega)(\Omega+\omega_0)^3}/2$; B, C are the time domain representations of $\tilde{B}, \tilde{C}$, and x^* stands for the complex conjugate of x. As in the case of the NLSE, the MI gain can be obtained by means of a linear stability analysis. It can be shown that (see the details in Ref. [22])

$$g_{\mathrm{MI}}(\Omega) = 2\left|\mathrm{Im}\left\{\sqrt{\left(\frac{\Delta k}{2}\right)^2 - \overline{\gamma}(\Omega)^2 P_0^2}\right\}\right|, \tag{10}$$

where

$$\Delta k = 2k_{\mathrm{P}} - k_{\mathrm{S}} - k_{\mathrm{AS}}, \tag{11}$$

$$\begin{cases} 2k_{\mathrm{P}} &= 2\gamma_0 P_0, \\ k_{\mathrm{S}} &= \beta(-\Omega) + 2\overline{\gamma}_{\mathrm{S}} P_0, \\ k_{\mathrm{AS}} &= \beta(+\Omega) + 2\overline{\gamma}_{\mathrm{AS}} P_0, \end{cases} \tag{12}$$

and the functions $\overline{\gamma}(\Omega)$, $\overline{\gamma}_{\mathrm{S}}(\Omega)$ and $\overline{\gamma}_{\mathrm{AS}}(\Omega)$ are defined as

$$\overline{\gamma}(\Omega) = \mathrm{Re}\left\{\sqrt[4]{\gamma(-\Omega)}\sqrt[4]{\gamma_0}\sqrt[4]{\gamma_0}\sqrt[4]{\gamma(+\Omega)}\right\}\sqrt[4]{1-(\Omega/\omega_0)^2}, \tag{13}$$

$$\overline{\gamma}_{\mathrm{S}}(\Omega) = \mathrm{Re}\left\{\sqrt[4]{\gamma(-\Omega)}\sqrt[4]{\gamma(-\Omega)}\sqrt[4]{\gamma_0}\sqrt[4]{\gamma_0}\right\}\sqrt{1-\Omega/\omega_0}, \tag{14}$$

$$\overline{\gamma}_{\mathrm{AS}}(\Omega) = \mathrm{Re}\left\{\sqrt[4]{\gamma_0}\sqrt[4]{\gamma_0}\sqrt[4]{\gamma(+\Omega)}\sqrt[4]{\gamma(+\Omega)}\right\}\sqrt{1+\Omega/\omega_0}, \tag{15}$$

where the subindices S and AS stand for the Stokes and anti-Stokes frequencies, respectively. Note that Eqs. 10-12 are similar to Eqs. 2-4 corresponding to the NLSE. The main difference lies in the way the nonlinearity is accounted for in Eqs. 13-15. It is easy to see, however, that Eqs. 10-15 reduce to those derived from the NLSE in the case $\gamma_0 > 0$ and $\gamma_1 = \gamma_{1,\mathrm{pc}}$.

For the sake of simplicity, let us once again assume that $\gamma(\Omega)$ varies linearly with frequency, *i.e.*, $\gamma(\Omega) = \gamma_0 + s\gamma_{1,\mathrm{pc}}\Omega$, and that $\beta(\Omega) = \beta_2\Omega^2/2$. In Fig. 2 we show different MI gain profiles obtained with the pcNLSE, using Eq. 10, the same waveguide and pump parameters as in Fig. 1, and for different s, namely 1, 3, 5, and 10, *i.e.*, a range that is encountered in the literature [20, 21, 26, 27]. Most remarkable, fora large s the COP disappears, leading to spectral narrowband gain regions not dependent on the pump power. Furthermore, MI gain lobes do not converge to the central frequency with increasing pump power, as predicted by the NLSE.

In order to obtain the geometry of the MI gain region, we proceed as in the previous case with the NLSE. From Eq. 10 we find that it is given by

$$R_{\mathrm{MI}} = \left\{(\Omega, P_0):\ \left[(\gamma_0 - \bar{\gamma}_{\mathrm{S}} - \bar{\gamma}_{\mathrm{AS}})^2 - \bar{\gamma}^2\right] P_0^2 - (\gamma_0 - \bar{\gamma}_{\mathrm{S}} - \bar{\gamma}_{\mathrm{AS}})\,\beta_2\Omega^2\,P_0 + \frac{\beta_2^2\Omega^4}{4} < 0\right\}, \tag{16}$$

where we have assumed that $\beta(\Omega) = \beta_2\Omega^2/2$ for the sake of clarity. Comparing Eq. 16 to Eq. 6 we find many similarities, and once again it is easy to show that both results are equivalent in the case of $\gamma_1 = \gamma_{1,\mathrm{pc}}$.

Proceeding analogously as it was done in the case of the NLSE, it can be shown that the pump power in the boundary is given by

$$P^{\mathrm{co}} = \frac{\beta_2\Omega^2}{2(\gamma_0 \pm \bar{\gamma} - \bar{\gamma}_{\mathrm{S}} - \bar{\gamma}_{\mathrm{AS}})}. \tag{17}$$

This expression is valid for arbitrary nonlinear profiles $\gamma(\Omega)$. Moreover, Fig. 2 also shows that Eq. 17 successfully delineates the contour of MI gain.

We may re-write Eq. 17 as

$$P^{\mathrm{co}} = \hat{P} \times \frac{\bar{\Omega}^2}{\mathrm{Re}\left\{\sqrt{1+s\bar{\Omega}}\right\}\sqrt{1+\bar{\Omega}} + \mathrm{Re}\left\{\sqrt{1-s\bar{\Omega}}\right\}\sqrt{1-\bar{\Omega}} \pm \mathrm{Re}\left\{\sqrt[4]{1-(s\bar{\Omega})^2}\right\}\sqrt[4]{1-\bar{\Omega}^2} - 1}, \tag{18}$$

where $\hat{P}$ is defined in Eq. 8. A remarkable feature of the geometry of the modulation instability gain as revealed by Eq. 18 is that the position and bandwidth of the MI gain do not depend

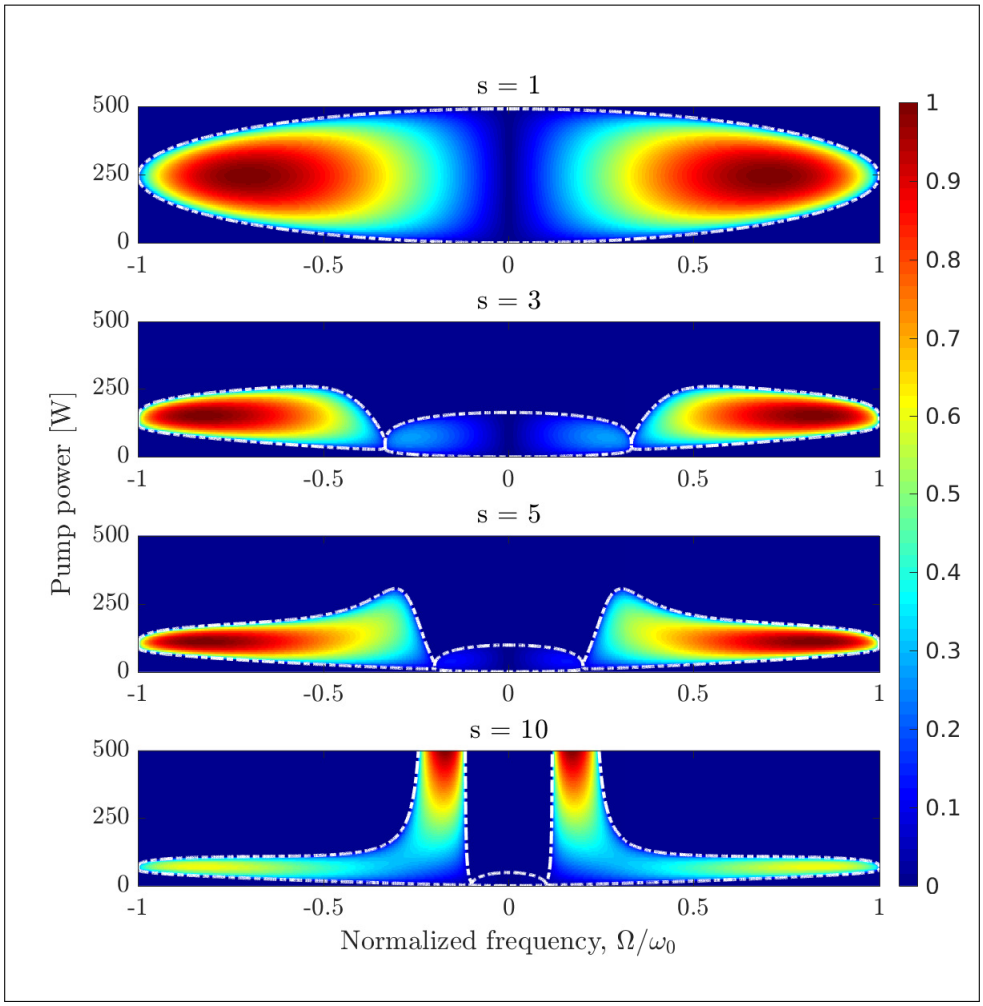

Fig. 2. MI gain profiles obtained with the pcNLSE. Waveguide parameters are the same as in Fig. 1. Different panels correspond to slopes s = 1, 3, 5, and 10, increasing from top to bottom. Dashed white lines show the contour of the gain region as given by Eq. 17. Observe the suppression of the power cutoff in the bottom panel.

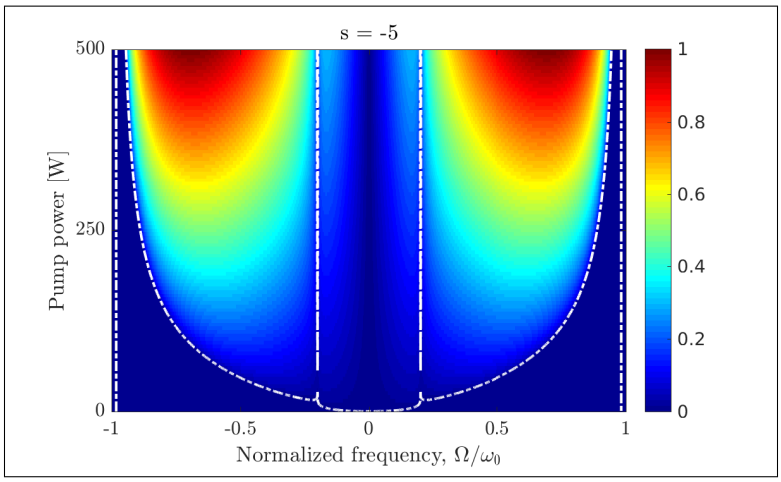

Fig. 3. MI gain profiles obtained with the pcNLSE. Waveguide parameters are the same as in the previous figures, but for a negative slope $s = -5$. Dashed white lines show the contour of the gain region as given by Eq. 17.

neither on the linear dispersion coefficient β_2 nor on the nonlinear parameter γ_0, but only on the nonlinear slope and the pump frequency.

It is interesting to compare Eq. 18 to Eq. 7. As it can be readily seen, the COP strongly depends on the sign of the SS parameter, unlike the behavior predicted in Ref. [15] and noted above for the case of the NLSE. In Fig. 3 we show the MI gain for a negative self-steepening parameter.

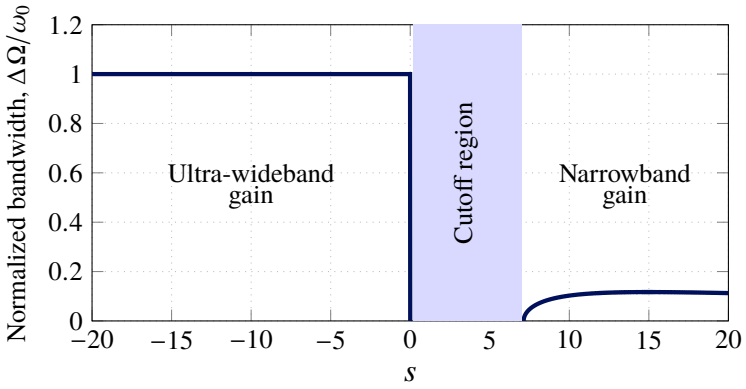

Fig. 4. Modulation instability gain bandwidth as a function of the slope of the nonlinear coefficient s, as obtained with the pcNLSE. Two markedly distinct regimes are observed: Ultra-wideband gain ($s < 0$) and narrowband gain ($s > s_0$). These are separated by a region of nonzero cutoff power (shaded blue).

A fruitful way of analyzing the influence of the slope of the nonlinear coefficient $\gamma(\Omega)$ is by focusing on the MI gain bandwidth for pump powers much greater than $\hat{P}$. Figure 4 shows the gain bandwidth as a function of the slope of the nonlinear coefficient, for both positive and negative values of s. Most notably, two markedly distinct regimes become apparent: An ultra-wideband regime (see Fig. 3) where the MI gain covers the whole available spectrum ($s < 0$) and a narrowband regime (for a set of positive values $s > s_0$) where the gain bandwidth is only a small fraction of the pump frequency. These two regimes are separated by an interval of positive

values of s where there exists a cutoff power lower than the pump power and, as such, there is no MI gain.

Figure 5 shows simulation results with the pcNLSE, performed with a fourth-order Runge-Kutta in the interaction picture method [28], for the propagation of a CW pump plus additive white Gaussian noise in a nonlinear waveguide. The pump power is $P_0 = 5000$ W at a wavelength $\lambda_0 = 5000$ nm, and a pump signal-to-noise ratio set to 120 dB. Waveguide constants are $\beta_2 = -0.1$ ps^2/km and $\gamma_0 = 1000$ W^{-1}km^{-1}. These values were purposely chosen to correspond to those typical of waveguides made of chalcogenide glasses, *i.e.*, transparent media in the mid IR. Note that self-steepening effects in this spectral region are expected to be augmented due to the lower pump frequencies involved and the high nonlinear coefficient of chalcogenide glass. Last, $s = 7.15 > s_0$ and the propagation length is $10L_{\mathrm{MI}}$, where the modulation instability characteristic length is $L_{\mathrm{MI}} = 1/\max(g_{\mathrm{MI}})$. The value of s was chosen to fall within the region of narrowband MI gain (see Fig. 4) and $P_0 \gg \hat{P} = 7.1$ W. Indeed, two regions of narrowband gain are clearly observed in the figure. Furthermore, note that the maximum COP for the chosen simulation parameters, as calculated with the NLSE (see Eqs. 7-8), is $P^{\mathrm{co}} = 0.3$ W; thus, according to the NLSE, the expected gain at 5000 W should be zero, in stark contrast with results obtained with the pcNLSE.

In order to portray the ultra-wideband regime, Fig. 6 shows simulation results with the same parameters as before, but with $s = -1$ (see Fig. 4). As predicted by Eq. 18, a broad and almost constant gain bandwidth is obtained over the whole available spectrum. The attentive reader might note a slight asymmetry present in the spectral density. Interestingly, this is a clear manifestation of MI as a degenerate four-wave mixing parametric process, as positive and negative frequencies 'receive' the exact same number of photons from the pump; however, the higher the photon frequency, the higher the energy, leading to the observed imbalance in the spectral density. As expected, this effect becomes more apparent in the case of a wide gain spectrum, and is not observable in the narrowband case (see Fig. 5).

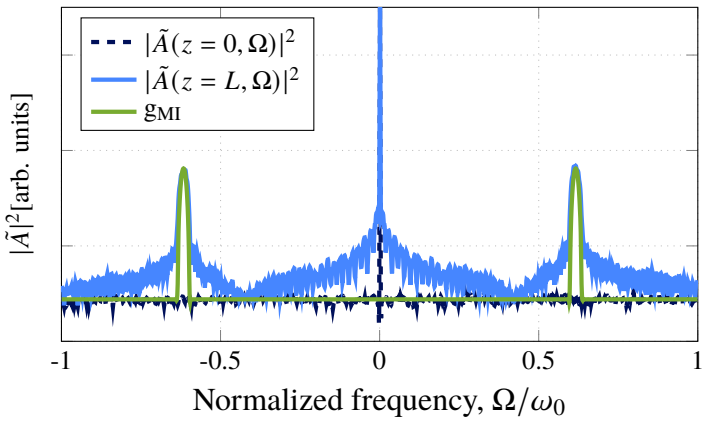

Fig. 5. Narrowband MI gain in the pcNLSE. Simulation results for a CW pump plus additive white Gaussian noise. Input (dashed blue line), output at a propagated length $L = 10L_{\mathrm{MI}}$ (solid light blue line), and MI gain profile (solid green line) are shown. Input signal parameters are $P_0 = 5000$ W, $\lambda_0 = 5000$ nm, and waveguide parameters are $\beta_2 = -0.1$ ps^2/km, $\gamma_0 = 1000$ W^{-1}km^{-1}, $s = 7.15$.

Results in Fig. 5 and Fig. 6 suggest a fundamentally different behavior when looking at the output of the waveguide in the time domain. Figure 7 shows the corresponding outputs for the narrowband (left) and the ultra-wideband (right) cases. The former exhibits a coherent train of pulses, while the latter shows the onset of jittery pulse formation.

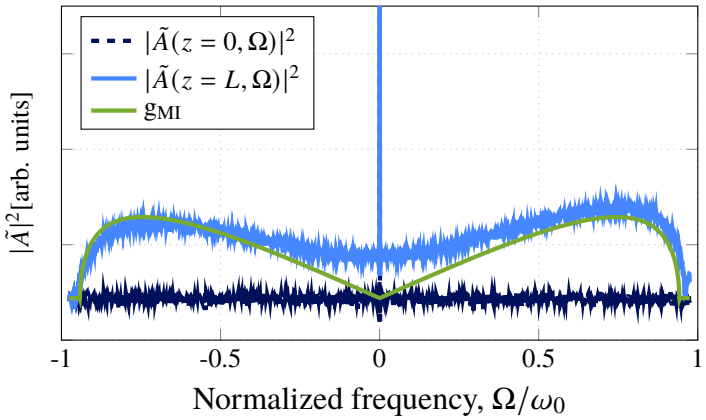

Fig. 6. Ultra-wideband MI gain in the pcNLSE. Simulation results for a CW pump plus additive white Gaussian noise. Input (dashed blue line), output at a propagated length $L = 10L_{MI}$ (solid light blue line), and MI gain profile (solid green line) are shown. Simulation parameters are the same as in Fig. 5 with $s = -1$.

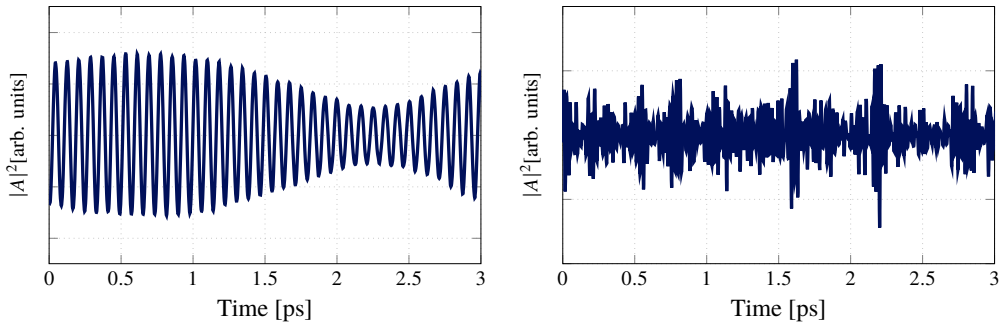

Fig. 7. Waveforms at the output of the waveguide corresponding to the narrowband (left) and the ultra-wideband (right) MI regimes of Figs. 5 and 6, respectively.

4. Conclusions

The nonlinear-Schrödinger equation (NLSE) is inadequate to model the propagation of pulses in waveguides with arbitrary frequency dependent nonlinearities. In particular, application of the NLSE may lead to incorrect results in the analysis of modulation instability.

Based on quantum-mechanical considerations, we have recently derived the photon-conserving NLSE (pcNLSE) which can be applied to arbitrary frequency dependent nonlinearities, such as those found in waveguides built with metamaterials.

In this paper, we studied the modulation-instability gain in the context of the pcNLSE and compared our results to those predicted by the NLSE. While results obtained with the NLSE are independent of the sign of the self-steepening parameter, the pcNLSE predicts a strong dependence. Most remarkably, the analysis based on the pcNLSE revealed unexpected and unique features such as regions where the MI-gain power cutoff is suppressed, leading to either narrowband or ultra-wideband modulation instability gain depending upon the sign of the SS parameter, and producing markedly different output waveforms. Finally, we believe these findings to be most relevant in the context of the design and optimization of mid-IR supercontinuum sources based on nonlinear metamaterial waveguides, where the pump wavelength and involved

spectral bandwidths call for the necessary inclusion of self-steepening in the analysis.

Disclosures

The authors declare no conflicts of interest.

References

1. A. Hasegawa and W. Brinkman, "Tunable coherent ir and fir sources utilizing modulational instability," IEEE J. Quantum Electron. **16**, 694–697 (1980).
2. D. Anderson and M. Lisak, "Modulational instability of coherent optical-fiber transmission signals," Opt. Lett. **9**, 468–470 (1984).
3. K. Tai, A. Hasegawa, and A. Tomita, "Observation of modulational instability in optical fibers," Phys. Rev. Lett. **56**, 135 (1986).
4. M. Potasek, "Modulation instability in an extended nonlinear Schrödinger equation," Opt. Lett. **12**, 921–923 (1987).
5. A. R. Seadawy, "Modulation instability analysis for the generalized derivative higher order nonlinear Schrödinger equation and its the bright and dark soliton solutions," J. Electromagn. Waves Appl. **31**, 1353–1362 (2017).
6. S. M. Hernandez, P. I. Fierens, J. Bonetti, A. D. Sánchez, and D. F. Grosz, "A geometrical view of scalar modulation instability in optical fibers," IEEE Photonics J. **9**, 1–8 (2017).
7. J. Bonetti, S. M. Hernandez, P. I. Fierens, and D. Grosz, "A higher-order perturbation analysis of the nonlinear Schrödinger equation," Commun. Nonlinear Sci. Numer. Simul. **72**, 152–161 (2019).
8. V. E. Zakharov and L. Ostrovsky, "Modulation instability: the beginning," Phys. D **238**, 540–548 (2009).
9. M. Saha and A. K. Sarma, "Solitary wave solutions and modulation instability analysis of the nonlinear Schrödinger equation with higher order dispersion and nonlinear terms," Commun. Nonlinear Sci. Numer. Simul. **18**, 2420–2425 (2013).
10. D. Anderson and M. Lisak, "Nonlinear asymmetric self-phase modulation and self-steepening of pulses in long optical waveguides," Phys. Rev. A **27**, 1393 (1983).
11. P. Shukla and J. J. Rasmussen, "Modulational instability of short pulses in long optical fibers," Opt. Lett. **11**, 171–173 (1986).
12. C. D. Angelis, G. Nalesso, and M. Santagiustina, "Role of nonlinear dispersion in the dynamics of induced modulational instability in kerr media," J. Opt. Soc. Am. B **13**, 848–855 (1996).
13. G. Xu, J. McNiff, A. Boardman, and B. Kibler, "Space–time evolution of optical breathers and modulation instability patterns in metamaterial waveguides," Wave Motion **93**, 102448 (2020).
14. A. Sánchez, N. Linale, J. Bonetti, and D. Grosz, "Modulation instability in waveguides doped with anisotropic nanoparticles," Opt. Lett. **45**, 3119–3122 (2020).
15. S. Wen, Y. Wang, W. Su, Y. Xiang, X. Fu, and D. Fan, "Modulation instability in nonlinear negative-index material," Phys. Rev. E **73**, 036617 (2006).
16. S. Wen, Y. Xiang, W. Su, Y. Hu, X. Fu, and D. Fan, "Role of the anomalous self-steepening effect in modulation instability in negative-index material," Opt. Express **14**, 1568–1575 (2006).
17. A. D. Sánchez, P. I. Fierens, S. M. Hernandez, J. Bonetti, G. Brambilla, and D. F. Grosz, "Anti-Stokes Raman gain enabled by modulation instability in mid-IR waveguides," J. Opt. Soc. Am. B **35**, 2828–2832 (2018).
18. K. Blow and D. Wood, "Theoretical description of transient stimulated Raman scattering in optical fibers," IEEE J. Quantum Electron. **25**, 2665–2673 (1989).
19. J. Bonetti, N. Linale, A. D. Sánchez, S. M. Hernandez, P. I. Fierens, and D. F. Grosz, "Modified nonlinear Schrödinger equation for frequency-dependent nonlinear profiles of arbitrary sign," J. Opt. Soc. Am. B **36**, 3139–3144 (2019).
20. S. Bose, A. Sahoo, R. Chattopadhyay, S. Roy, S. K. Bhadra, and G. P. Agrawal, "Implications of a zero-nonlinearity wavelength in photonic crystal fibers doped with silver nanoparticles," Phys. Rev. A **94**, 043835 (2016).
21. F. R. Arteaga-Sierra, A. Antikainen, and G. P. Agrawal, "Soliton mitosis across a zero-nonlinearity wavelength in photonic crystal fibers," in *Frontiers in Optics,* (Optical Society of America, 2017), pp. FTu5A–2.
22. N. Linale, J. Bonetti, A. D. Sánchez, S. Hernandez, P. I. Fierens, and D. Grosz, "Modulation instability in waveguides with an arbitrary frequency-dependent nonlinear coefficient," Opt. Lett. **45**, 2498–2501 (2020).
23. T. Brabec and F. Krausz, "Intense few-cycle laser fields: Frontiers of nonlinear optics," Rev. Mod. Phys. **72**, 545 (2000).
24. J. M. Dudley, G. Genty, and S. Coen, "Supercontinuum generation in photonic crystal fiber," Rev. Mod. Phys. **78**, 1135–1184 (2006).
25. G. Agrawal, *Nonlinear Fiber Optics*, Optics and Photonics (Academic Press, 2012).
26. N. C. Panoiu, X. Liu, and R. M. Osgood, "Nonlinear dispersion in silicon photonic wires," in *2008 Conference on Lasers and Electro-Optics and 2008 Conference on Quantum Electronics and Laser Science,* (IEEE, 2008), pp. 1–2.
27. N. C. Panoiu, X. Liu, and R. M. Osgood Jr, "Self-steepening of ultrashort pulses in silicon photonic nanowires," Opt. Lett. **34**, 947–949 (2009).
28. J. Hult, "A fourth-order Runge–Kutta in the interaction picture method for simulating supercontinuum generation in optical fibers," J. Light. Technol. **25**, 3770–3775 (2007).